Ordering state and magnetism in highly doped manganites studied with magnetization and ESR measurements



2008 J. Phys.: Condens. Matter 20 125214

(http://iopscience.iop.org/0953-8984/20/12/125214)

J. Phys.: Condens. Matter **20** (2008) 125214 (7pp) doi:10.1088/0953-8984/20/12/125214

# Ordering state and magnetism in highly doped manganites studied with magnetization and ESR measurements

**Langsheng Ling[1], Jiyu Fan[1], Li Pi[1,2], Yue Ying[1], Shun Tan[1] and Yuheng Zhang[1]**

[1] National High Magnetic Field Laboratory, University of Science and Technology of China, Hefei 230026, People's Republic of China
[2] Hefei National Laboratory for Physical Sciences at the Microscale, University of Science and Technology of China, Hefei 230026, People's Republic of China

E-mail: pili@ustc.edu.cn and zhangyh@ustc.edu.cn

Received 2 October 2007, in final form 22 January 2008
Published 27 February 2008
Online at stacks.iop.org/JPhysCM/20/125214

**Abstract**
The electrical and magnetic properties of $Ln_{0.4}Ca_{0.6}MnO_3$ compositions (Ln = La, Pr, Nd, Sm) have been investigated. The effect of $\langle r_A \rangle$ on the charge-ordering behavior of the manganites is considered to be profound. The charge-ordering temperature $T_{CO}$ increases with decreasing $\langle r_A \rangle$, the antiferromagnetic charge-ordering state transforms from long-range into local short-range ordering and the magnetic behaviors for Ln = La, Pr, Nd, Sm are all different. Through the $M$–$T$, $M$–$H$, and electron spin resonance measurements, it is found that the magnetization in $M$–$T$ curves comes from the paramagnetic contribution of disordered Mn ions at the B-site and magnetic ions at the A-site. The rise of $T_{CO}$ is attributed to the fact that $e_g$ electrons are localized by decreasing $\langle r_A \rangle$, and the different behavior of $M$–$T$ curves below $T_{CO}$ originates from the number of remaining spin disordered Mn ions after the formation of the charge-ordering phase in the manganites.

## 1. Introduction

Manganites of the $ABO_3$ type have attracted much attention from researchers in recent years due to their fascinating properties such as colossal magnetoresistance, charge ordering, and their potential for applications [1]. Decades of research have allowed us to completely understand the full range of ordering phases that occur in the $R_{1-x}A_xMnO_3$ perovskites (R = La, Pr, Nd and A = Ca, Sr, Ba) [2]. For a sample with $x \leqslant 0.5$, complex competition occurs among ferromagnetic (FM), paramagnetic (PM), and antiferromagnetic (AFM) phases. In this regime, inhomogeneous phase separation (PS) gives rise to the well-known colossal magnetoresistance (CMR) effect [3–7]. On the other hand, highly doped manganites with $x \geqslant 0.5$ display orbital and charge order with an antiferromagnetic ground state below the charge-ordering (CO) temperature $T_{CO}$ [8, 9].

Recently, there have been a number of reports on the fact that the reduction of particle size has influence on the properties of manganites, especially charge ordering [10–15]. Moreover, the properties of manganites are not only sensitive to the manganese valency, but are also strongly affected by chemical factors such as average cationic radius $\langle r_A \rangle$ in the A-site [16–18] and A-site cationic size mismatch [19, 20] quantified by $\sigma^2 = \sum x_i r_i^2 - \langle r_A \rangle^2$ ($x_i$ is the fractional occupancy of A-site ions, and $r_i$ is the corresponding ionic radius) [19]. For instance, when the hole concentration is kept constant in the $Mn^{3+}$ rich FM compositions, it has been shown that the decrease of $\langle r_A \rangle$ tends to diminish the Mn–O–Mn angle, which consequently reduces the bandwidth ($W$) and $T_C$ [17]. In contrast, a small $\langle r_A \rangle$ value is required for the appearance of CMR in $Mn^{4+}$-rich manganites [21]. Finally, whatever the values of $\langle r_A \rangle$ and manganese valency, increase in $\sigma^2$ tends to suppress the magnetic interactions, FM or AFM, and destabilize CO [19, 20]. These behaviors show the great complexity of the relationships between the chemical factors ($\langle r_A \rangle$, $\sigma^2$, carrier nature, and concentration) and the magnetotransport properties of manganites.

Charge ordering in the manganites is governed by the width of the $e_g$ band which is directly determined by the

 

weighted average radius of A-site cations $\langle r_A \rangle$, or the tolerance factor $t$. This is because a distortion of the Mn–O–Mn bond angle affects the transfer interaction of the $e_g$ conduction electrons (holes) [22]. A comparative study of the nature of the charge-ordered state has been carried out in hole-doped and electron-doped manganites, which revealed that the electronic structures of the two manganites have basic differences [23]. Damay *et al* investigated the relationships between Curie temperature $T_C$ (Neél temperature $T_N$) and average ionic radius of the A-site cations in manganite perovskites $Ln_{0.5}Sr_{0.5}MnO_3$ (Ln = Gd, Sm, Y, Pr, La). Their results show that $T_C$ increases dramatically as the $\langle r_A \rangle$ increases, ranging from 110 K with an ionic radius of 1.225 Å to 310 K with an ionic radius of 1.263 Å, while $T_N$ is almost constant and ranges from 135 to 145 K for ionic radii ranging from 1.228 to 1.264 Å [24]. Arulraj *et al* have investigated the structure as well as the electrical and magnetic properties of $Ln_{0.5}Ca_{0.5}MnO_3$ compositions (Ln = Nd, Sm, Gd, and Dy) wherein $\langle r_A \rangle$ varies over the range 1.17–1.13 Å. Their results show that the lattice distortion index, $D = \sum |(a_i - a)|/3a_i$, and charge-ordering transition temperature, $T_{CO}$, of the manganites increase with decreasing $\langle r_A \rangle$ [25].

These observations revealed that $\langle r_A \rangle$ has a profound effect on the charge-ordering behavior of manganites. However, previous studies mostly focused on the half-doped manganites which locate at the boundary in the phase diagram. Although early researchers reported the relationship between $T_{CO}$ and $\langle r_A \rangle$, they ignored the discrepancy in the behavior of $M$–$T$ curves. The reason for these different behaviors and the physics involved has not been clarified, so further investigation for A-site average radius will provide interesting insights. In this paper we systemically study the electrical and magnetic properties of $Ln_{0.4}Ca_{0.6}MnO_3$ manganites (Ln = La, Pr, Nd, Sm) which exhibit a charge-ordering state with a relatively high $T_{CO}$. The reason why we choose $Ln_{0.4}Ca_{0.6}MnO_3$ is to keep away from the phase boundary of FM and AFM, while avoiding the considerable magnetic fluctuation. The results indicate that with decreasing $\langle r_A \rangle$ from 1.19 to 1.16 Å the charge-ordering temperature $T_{CO}$ increases, and the AFM charge-ordering state transforms from a long-range into a local short-range ordering state. The different behavior of $M$–$T$ curves below $T_{CO}$ is mainly attributed to the number of remaining spin-disordered Mn ions after the formation of the charge-ordering phase.

## 2. Experiment

Polycrystalline $Ln_{0.4}Ca_{0.6}MnO_3$ (Ln = La, Pr, Nd, Sm) samples were prepared by a traditional solid-state reaction method. Stoichiometric quantities of high-purity oxides of the rare earths, $CaCO_3$, and $MnO_2$ were thoroughly mixed and ground, then preheated at 1173 K for 24 h. With intermediate grinding, they reacted at 1673 K for 24 h. After the samples pressed were into pellets, a final sintering was carried out at 1673 K for 48 h. The structure and phase purity of the as-prepared samples were checked by powder x-ray diffraction (XRD) using Cu K$\alpha$ radiation at room temperature. The XRD patterns prove that the structure of all samples are single-phase with an orthorhombic perovskite structure. Magnetization measurements were performed using a SQUID magnetometer (Quantum Design MPMS). Resistivity properties were measured by the standard four-probe method. Electron spin resonance (ESR) measurement was also carried out on the samples using a JES-FA200 spectrometer at 9.06 GHz.

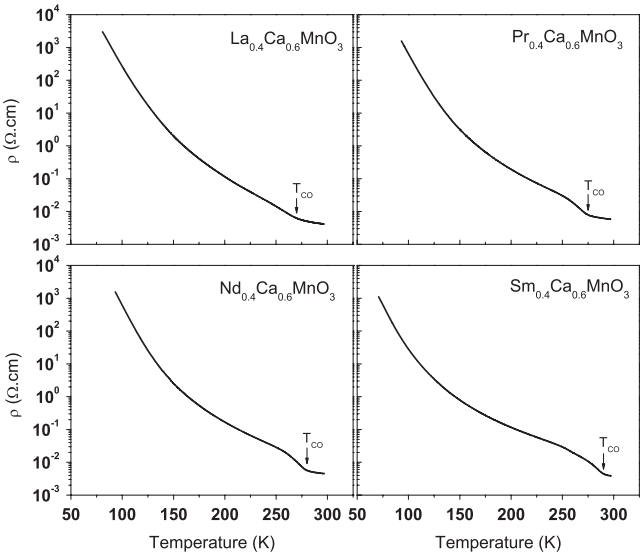


**Figure 1.** Temperature dependence of the resistivity of $Ln_{0.4}Ca_{0.6}MnO_3$ (Ln = La, Pr, Nd, Sm).

## 3. Results and discussion

The resistivity of $Ln_{0.4}Ca_{0.6}MnO_3$ (Ln = La, Pr, Nd, Sm) as a function of temperature is presented in figure 1. The resistivity is relatively small (about $10^{-3}$ Ω cm) at room temperature, while it rises rapidly with cooling and reaches $10^3$ Ω cm at the lowest temperature. A charge-ordering transition in manganites is often characterized as a change of slope in the resistivity curve. The charge-ordering temperature $T_{CO}$ of $Ln_{0.4}Ca_{0.6}MnO_3$ (Ln = La, Pr, Nd, Sm) is marked by an arrow in figure 1, at which point the system undergoes a transition from a charge-disordering to a charge-ordering state. We have summarized the lattice parameters, $\langle r_A \rangle$, $t$, and $T_{CO}$ in table 1. The weighted average radius of the A-site cations $\langle r_A \rangle$ ($\langle r_A \rangle = \sum x_i r_i$) and tolerance factor $t$ ($t = (\langle r_A \rangle + \langle r_O \rangle)/\sqrt{2}(\langle r_B \rangle + \langle r_O \rangle)$) are calculated using nine-coordinated ionic radii given by Shannon [26]. It is found that $T_{CO}$ increases with the decrease of $\langle r_A \rangle$. The tolerance factor $t$, which is used to define the mismatch between the A-site and B-site, decreases smoothly with $\langle r_A \rangle$. This indicates that the distortion of $MnO_6$ octahedra increases with Ln changing from La to Sm. It is well known that $\langle r_A \rangle$ directly affects the Mn–O–Mn angle, bandwidth $W$, and the average Mn–O distance in the manganites. According to Arulraj's work [25] it can be inferred that the Mn–O–Mn angle and bandwidth $W$ decreases with $\langle r_A \rangle$, while the average Mn–O distance increases smoothly with the $\langle r_A \rangle$ in the present range. These changes weaken the hopping integral of $e_g$ electrons, and tend to facilitate

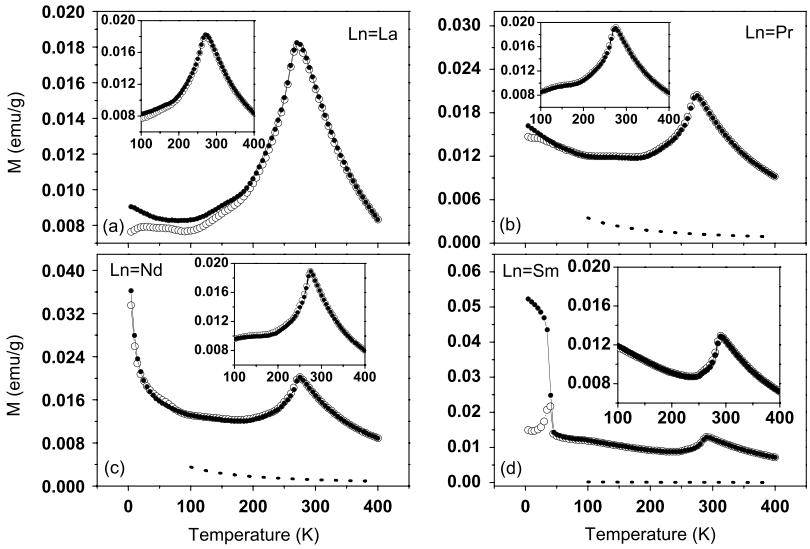


**Figure 2.** Temperature dependence of magnetization (empty circle for ZFC; solid circle for FC) in $Ln_{0.4}Ca_{0.6}MnO_3$ (Ln = La, Pr, Nd, Sm) and the calculated magnetization (dotted line) of Ln ions (Ln = Pr, Nd, Sm). The inset shows the temperature dependence of magnetization after subtracting the PM contribution of Ln ions (Ln = Pr, Nd, Sm).

**Table 1.** Lattice parameters, $\langle r_A \rangle$, $t$ factor, and $T_{CO}$ of $Ln_{0.4}Ca_{0.6}MnO_3$ manganites.

| | | | | | | $T_{CO}$ (K) | | |
|---|---|---|---|---|---|---|---|---|
| Ln | $a$ (Å) | $b$ (Å) | $c$ (Å) | $\langle r_A \rangle$ (Å) | $t$ | $M$–$T$ | $\rho$–$T$ | ESR |
| La | 5.4057 | 7.5951 | 5.4022 | 1.1944 | 0.9421 | 270 | 270 | 270 |
| Pr | 5.3951 | 7.5893 | 5.3889 | 1.1796 | 0.9285 | 275 | 275 | 280 |
| Nd | 5.3808 | 7.5673 | 5.3747 | 1.1732 | 0.9226 | 275 | 280 | 280 |
| Sm | 5.3560 | 7.5325 | 5.3915 | 1.1608 | 0.9112 | 290 | 290 | 300 |

the localization of separate $Mn^{3+}$ and $Mn^{4+}$ ions through the formation of polarons, which cause the increases in $T_{CO}$. Our experiment results are in agreement with a previous study [25].

Figure 2 shows the temperature dependence of magnetization, determined in warming-up processes with an applied field $H = 0.01$ T after the samples were first cooled down to 4 K either with 0.01 T (FC) or without any magnetic field (ZFC). All samples experience a magnetic transition from PM to AFM with temperature cooling, and a broad transition peak occurs at the temperature which is defined as the charge-ordering temperature $T_{CO}$ (see table 1). It can also be seen that $T_{CO}$ increases with decreasing $\langle r_A \rangle$. Generally speaking, the charge-ordering state in manganites is associated with insulating and antiferromagnetic (or paramagnetic) behavior. The peak of magnetization at $T_{CO}$ indicates the charge-ordering transition of the manganites, where the double exchange interaction is suppressed due to the localization of the charge carriers, producing a large drop in the magnetization. Here there are two further issues worth considering. First, the drop of magnetization below $T_{CO}$ in $M$–$T$ curves is weakened with decreasing $\langle r_A \rangle$. It should be pointed out that the drop of magnetization means from its maximum value at $T_{CO}$ to its lowest value below $T_{CO}$. Second, the behavior of $M$–$T$ curves below $T_{CO}$ for Ln = La, Pr, Nd, Sm is different for each Ln. In order to clarify these issues, the origin of the magnetization should be determined first.

The magnetization in $M$–$T$ curves could come from PM or FM. To distinguish these cases, the micro- and macro-magnetism of the samples were investigated through ESR and $M$–$H$ measurements. ESR spectra are shown in figure 3. Clearly, only the paramagnetic signals with $g \approx 2$ were detected in $Ln_{0.4}Ca_{0.6}MnO_3$ manganites [27, 28]. Throughout the temperature range in which we observe the EPR signal, it is found that the EPR spectra from the powder samples are Lorentzian in shape, similar to those from powder samples of $Pr_{1-x}Ca_xMnO_3$ [28, 29]. With decreasing temperature, the intensity of the PM signal increases first, reaches a maximum at a certain temperature, and then decreases. Since there is no ferromagnetic signal with $g < 2$, the above results indicate that the decrease of intensity of the PM signal should be attributed to the formation of the AFM phase. In the temperature dependence of double integrated intensities (DIN) shown in figure 4, a noticeable peak occurs in all samples and the corresponding temperatures are defined as $T_{CO}$ [30] which are also summarized in table 1. Figure 5 presents the temperature dependence of linewidth. The linewidth $\Delta H_{PP}$ was straightforwardly deduced from the peak-to-peak distance between the maximum and the minimum of the ESR spectra. As shown in figure 5, the linewidth shows a non-monotonic behavior. It decreases as the temperature is lowered from 370 K down to the temperature of $T_{CO}$ and then increases with further cooling. The increase of linewidth above $T_{CO}$ can be interpreted in terms of spin–lattice relaxation [31, 32]. Figure 6 shows the temperature dependence of the $g$-factor. It can be seen that the $g$-factor for the Ln = La composition exhibits remarkable differences from the others. The $g$ values show a monotonic increase as the temperature is reduced from 370 K in the La doped compound, showing a crossover from less than the free electron $g$ value $g_e$ to a value larger than $g_e$. This behavior is similar to that of PCMO-e [29]. The $g$-factor of Ln = Pr, Nd, and Sm compositions shows a non-monotonic behavior. It also can be noticed that the magnitude

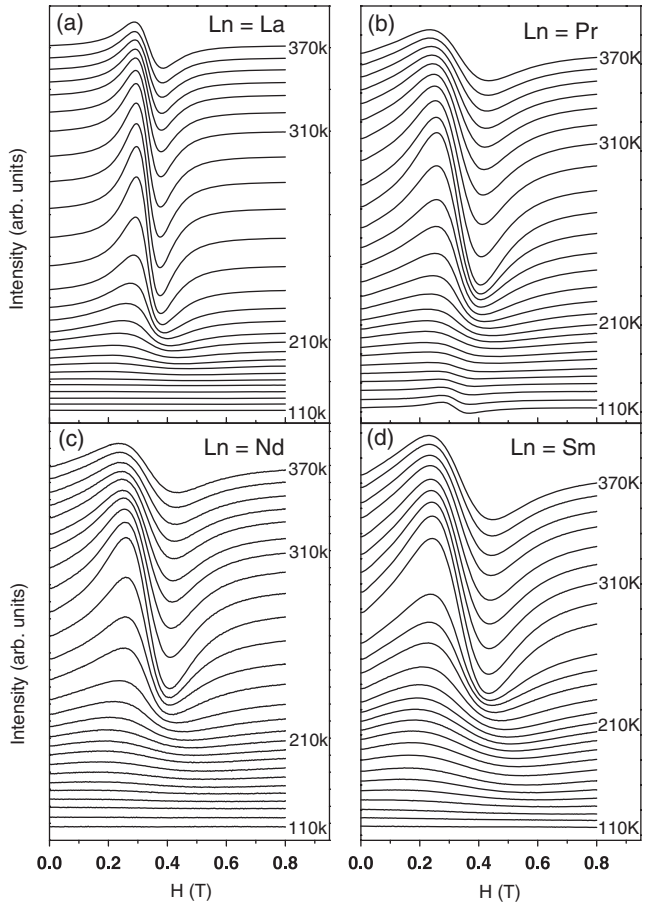


**Figure 3.** Temperature dependence of ESR signal for $Ln_{0.4}Ca_{0.6}MnO_3$ (Ln = La, Pr, Nd, Sm).

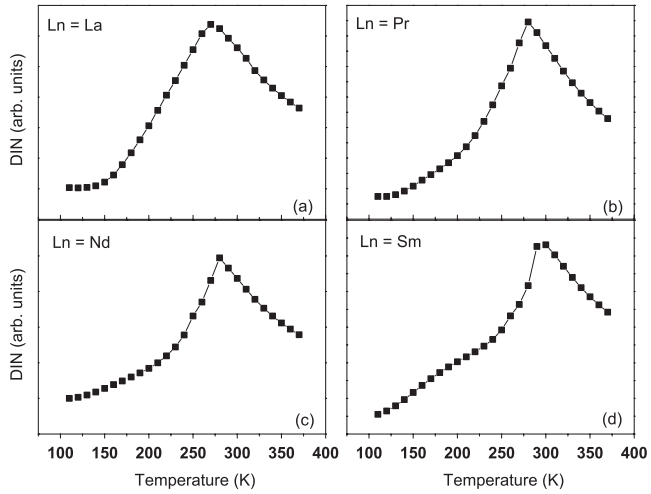


**Figure 4.** Temperature dependence of double integrated intensities (DIN) for the samples.

of $g$ is less than $g_e$ throughout the temperature range. In spite of the existence of the AFM phase, AFM signals have not been detected in the spectra. This may be because the coupling of AFM is too strong to be detected in the ESR measurement. That is, a PM–AFM phase transition has taken place at temperatures below $T_{CO}$. The magnetic behavior around $T_{CO}$ should stem from the competition between PM and AFM.

In order to clarify further the origin of magnetization, the $M$–$H$ relationship has been measured at typical temperatures as shown in figure 7. Apart from those for Ln = Nd at the lowest temperature 4 K and Ln = Sm at $T \leqslant 40$ K, which are shown in the inset of figures 7(c) and (d), the $M$–$H$ curves show a straight line indicating PM behavior. It has also been noticed that the slope of the $M$–$H$ curves changes with temperature variation and this behavior is coincident with the $M$–$T$ curves. This result indicates the existence of an AFM phase. At the same time, the AFM coupling is so strong as to remain stable under a magnetic field as high as 6 T, which also discloses the reason why we cannot detect the AFM signal in ESR measurement. As for Ln = Sm, only few FM phases occur and the PM phase is still in the majority, as shown in the inset of figure 7(d). Based on the above experimental results, it can be concluded that the magnetization in $M$–$T$ curves originates from the PM contribution.

In $Ln_{0.4}Ca_{0.6}MnO_3$ manganites, the magnetic ions at the A-site and Mn ions at the B-site could make a contribution to paramagnetism. In order to verify their contribution, the magnetization of PM for Ln (Ln = Pr, Nd, Sm) ions at the A-site in $Ln_{0.4}Ca_{0.6}MnO_3$ manganites per gram is calculated by Langevin theory:

$$M = NJg_J\mu_B B_J(x)$$

$$B_J(x) = \frac{2J+1}{2J}\coth\frac{2J+1}{2J}x - \frac{1}{2J}\coth\frac{1}{2J}x,$$

$$x = Jg_J\mu_B B/k_B T$$

where $B_J(x)$ is the Brillouin function, $N$ is the number of Ln ions and $J$ is the quantum number of angular moment. The dotted line in figure 2 shows theoretical $M$–$T$ relation at $T > 100$ K for magnetic ions at the A-site. The inset in figure 2 shows the temperature dependence of net magnetization, in which the calculated contribution of magnetic ions at the A-site has been subtracted from experimental result at high temperature ($T > 100$ K). It can be seen that the charge-ordering behavior remains stable, which indicates that the magnetism of magnetic ions at the A-site has no effect on charge-ordering in the manganites regardless of different magnetic moments. This result is reasonable since the magnetic interactions of the 4f ions are much weaker (the ordering temperature is usually <10 K) than those of the Mn ions. It is clearer in the inset of figure 2 that the drop of magnetization below $T_{CO}$ is weakened with decreasing $\langle r_A\rangle$. It should be emphasized that for Ln = Sm with small $\langle r_A\rangle$, the net magnetization decreases to the lowest value then increases upon cooling after the formation of the AFM-CO state. Since the contribution of magnetic ions at the A-site has been subtracted, the increase of net magnetization could only be attributed to the PM behavior of residual spin-disordered Mn ions after the formation of the AFM-CO state. And the different behavior of $M$–$T$ curves below $T_{CO}$ should also arise mainly from those spin-disordered Mn ions.

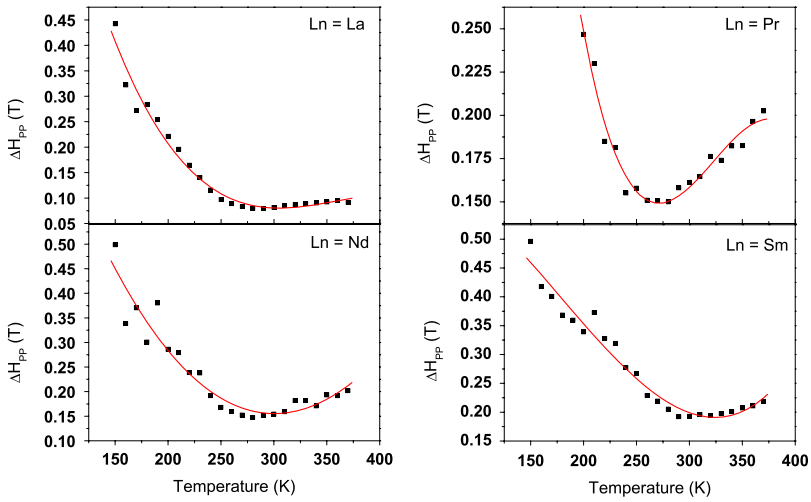


**Figure 5.** The variation of the linewidth $\Delta H_{PP}$ as a function of temperature for the samples (the lines are guides for the eye). (This figure is in colour only in the electronic version)

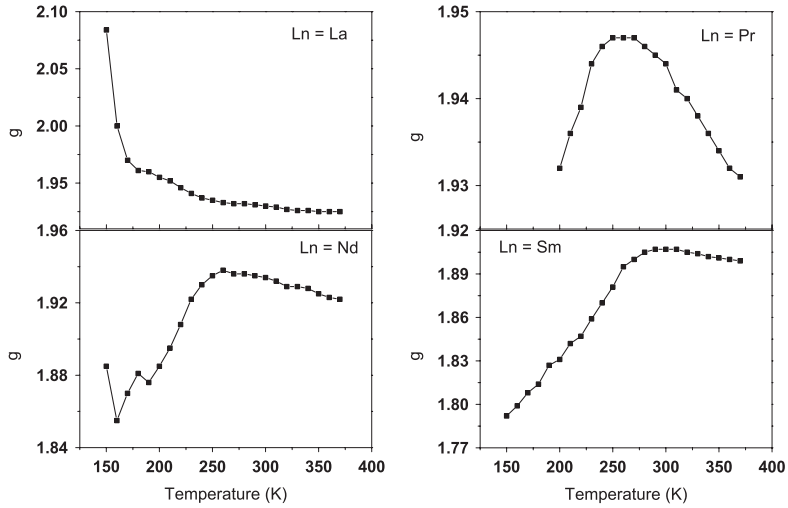


**Figure 6.** The temperature dependence of the $g$-factor for the samples.

Here, a question may be raised: why is it concluded that the relative change of DIN of ESR spectra following from figure 4(d) is different from the $M$–$T$ relation in the inset of figure 2(d) for Sm compositions. This experimental result should not be due to the formation of AFM phase. Though the DIN of ESR spectra could decrease with the formation of AFM phase and the AFM phase could still have a static susceptibility, the increase of magnetization with temperature cooling below 250 K in the inset of figure 2(d) should not originate from the AFM contribution. We suppose that the abnormal drop of DIN may result from the ferromagnetic superexchange interaction between the residual neighboring $Mn^{3+}$ and $Mn^{4+}$ ions, which favors the parallel spin configuration. This spin configuration still makes a contribution to the $M$–$T$ curve with cooling, but cannot be detected in the ESR spectrum. This is the reason why $M$–$T$ and DIN curves behave in an opposite fashion below $T_{CO}$.

These results imply that the region transformed into the AFM-CO state becomes smaller with decreasing $\langle r_A \rangle$. That is the AFM-CO state transfers from long-range ordering to local short-range ordering with decreasing $\langle r_A \rangle$. The absence of long-range magnetic order and the onset of short-range AFM order in $Y_{0.5}Ca_{0.5}MnO_3$ with a very small $\langle r_A \rangle$ have been investigated in previous work [33]. Moreover, Raveau *et al* revealed that the ruthenium doping of electron-doped manganites $Ln_{0.4}Ca_{0.6}MnO_3$ tends to weaken the charge ordering and to induce ferromagnetism and metallicity at low temperature [34]. We propose the following explanation for the experiment results. As mentioned previously, the tolerance factor $t$ decreases smoothly with $\langle r_A \rangle$. This indicates that the distortion of $MnO_6$ octahedra increases with Ln changing from La to Sm, which may result in the collapse of the long-range ordering state and the formation of a short-range ordering state with higher $T_{CO}$.

Based on the aforementioned results, we suggest the following interpretation for the system magnetism. The magnetic behavior around $T_{CO}$ is determined by $\langle r_A \rangle$ instead of the magnetism of A-site ions. Below $T_{CO}$, AFM coupling starts

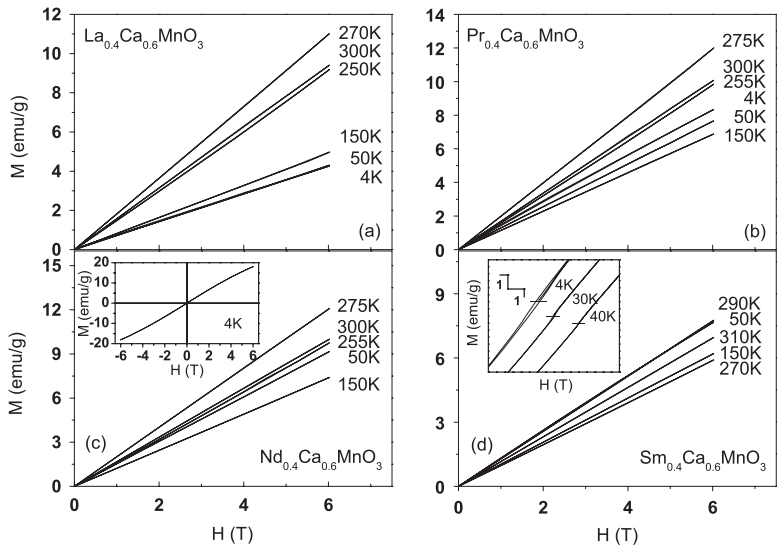


**Figure 7.** Magnetic field dependence of magnetization for $Ln_{0.4}Ca_{0.6}MnO_3$ (Ln = La, Pr, Nd, Sm) at typical temperatures.

to form and a PM–AFM phase transition takes place. However, due to the diminution of $\langle r_A \rangle$, the region of the AFM phase shrinks. Thus the number of residual spin-disordered Mn ions increases and dominates the magnetic behavior below $T_{CO}$. It is natural to expect that the more spin-disordered Mn ions exist, the stronger the magnetization will appear at low temperature. This is the reason responsible for the different behavior of $M$–$T$ curves from Ln = La with large $\langle r_A \rangle$ to that of Ln = Sm with small $\langle r_A \rangle$. For Ln = La, when $T < 100$ K the magnetization remains almost unchangeable, which indicates that the majority of Mn ions in the manganite establish AFM coupling and transfer into the AFM phase. While for Ln = Sm, only a fraction of Mn ions in the manganite form AFM coupling and the residual spin-disordered Mn ions result in the rapid increase of magnetization with cooling. After a careful investigation of $M$–$H$ curves in figure 7(d), it is found that there are very small hysteresis loops at 4, 30, and 40 K, which indicate the existence of a small FM region under the PM matrix. This small FM phase below 40 K should originate from the superexchange interaction among the residual $Mn^{3+}$ and $Mn^{4+}$ ions. This result is represented in $M$–$T$ curves. From figure 2(d) it can be seen that magnetization drops suddenly below 40 K in the ZFC curve while it rises rapidly in the FC curve, which is the typical 'λ' phase transition of an FM cluster glass state [35–38]. Finally, $\langle r_A \rangle$ for Ln = Pr is larger than that for Ln = Nd. Therefore, there are fewer residual spin-disordered Mn ions and magnetization increases more slowly with temperature cooling for Ln = Pr than for Ln = Nd.

## 4. Conclusion

The electrical and magnetic properties of $Ln_{0.4}Ca_{0.6}MnO_3$ compositions (Ln = La, Pr, Nd, Sm) have been investigated. The effect of $\langle r_A \rangle$ on the charge-ordering behavior of the manganites is seen to be particularly profound. The experimental results indicate that the charge-ordering temperature $T_{CO}$ increases with decreasing $\langle r_A \rangle$. The distortion of $MnO_6$ octahedra increases with decreasing $\langle r_A \rangle$, which may result in the collapse of the long-range ordering state and the formation of a short-range ordering state with higher $T_{CO}$. The different behavior of $M$–$T$ curves below $T_{CO}$ originates from the number of remaining spin-disordered Mn ions after the formation of the charge-ordering state in the manganites.

## Acknowledgments

This work is supported by National Natural Science Foundation of China through grant nos. 10334090, 10504029, and the State Key Project of Fundamental Research, China, no. 2007CB925001.

## References

[1] Rao C N R and Raveau B (ed) 1998 *Colossal Magnetoresistance* (Singapore: World Scientific)
[2] Salamon M B and Jaime M 2001 *Rev. Mod. Phys.* **73** 583
[3] Jin S, Tiefel T H, McCormack M, Fastnacht R A, Ramesh R and Chen L H 1994 *Science* **264** 413
[4] Dagotto E, Hotta T and Moreo A 2001 *Phys. Rep.* **344** 1
[5] Fäth M, Freisem S, Menovsky A A, Tomioka Y, Aarts J and Mydosh J A 1999 *Science* **285** 1540
[6] Biswas A and Das I 2007 *Appl. Phys. Lett.* **91** 013107
[7] Sen C, Alvarez G and Dagotto E 2007 *Phys. Rev. Lett.* **98** 127202
[8] van den Brink J, Khaliullin G and Khomskii D 1999 *Phys. Rev. Lett.* **83** 5118
[9] Radaelli P G, Cox D E, Marezio M and Cheong S W 1997 *Phys. Rev.* B **55** 3015
[10] Lu C L, Dong S, Wang K F, Gao F, Li P L, Lv L Y and Liu J-M 2007 *Appl. Phys. Lett.* **91** 032502
[11] Gao F, Li P L, Weng Y Y, Dong S, Wang L F, Lv L Y, Wang K F, Liu J-M and Ren Z F 2007 *Appl. Phys. Lett.* **91** 072504
[12] Dong S, Gao F, Wang Z Q, Liu J-M and Ren Z F 2007 *Appl. Phys. Lett.* **90** 082508
[13] Biswas A, Das I and Majumdar C 2005 *J. Appl. Phys.* **98** 124310
[14] Biswas A and Das I 2007 *J. Appl. Phys.* **102** 064303
[15] Biswas A and Das I 2006 *Phys. Rev.* B **74** 172405

[16] Mahesh R, Mahendiran R, Raychaudhuri A K and Rao C N R 1995 *J. Solid State Chem.* **114** 297
Mahesh R, Mahendiran R, Raychaudhuri A K and Rao C N R 1995 *J. Solid State Chem.* **120** 204
[17] Hwang H Y, Cheong S W, Radaelli P G, Marezio M and Batlogg B 1995 *Phys. Rev. Lett.* **75** 914
[18] Maignan A, Simon Ch, Caignaert V and Raveau B 1995 *Solid State Commun.* **96** 623
[19] Rodriguez-Martinez L M and Attfield J P 1996 *Phys. Rev.* B **54** 15622
[20] Damay F, Martin C, Maignan A and Raveau B 1997 *J. Appl. Phys.* **82** 6181
[21] Maignan A, Martin C, Damay F and Raveau B 1998 *Chem. Mater.* **10** 950
[22] Vogt T, Cheetham A K, Mahendiran R, Raychaudhuri A K, Mahesh R and Rao C N R 1996 *Phys. Rev.* B **54** 15303
[23] Parashar S, Sarathy K V, Vanitha P V, Raju A R and Rao C N R 2001 *J. Phys. Chem. Solids* **62** 1387
[24] Damay F, Maignan A, Martin C and Raveau B 1997 *J. Appl. Phys.* **81** 1372
[25] Arulraj A, Santhosh P N, Gopalan R S, Guha A, Raychaudhuri A K, Kumar N and Rao C N R 1998 *J. Phys.: Condens. Matter* **10** 8497
[26] Shannon R D 1976 *Acta Crystallogr.* A **32** 751
[27] Autret C, Gervais M, Gervais F, Raimboux N and Simon P 2004 *Solid State Sci.* **6** 815
[28] Gupta R, Joshi J P, Bhat S V, Sood A K and Rao C N R 2000 *J. Phys.: Condens. Matter* **12** 6919
[29] Joshi J P, Sarathy K V, Sood A K, Bhat S V and Rao C N R 2004 *J. Phys.: Condens. Matter* **16** 2869
[30] Autret C, Gervais M, Zaghrioui M, Roger S, Gervais F, Raimboux N and Simon P 2005 *Eur. Phys. J.* B **47** 207
[31] Shengelaya A, Zhao G-M, Keller H and Muller K A 1996 *Phys. Rev. Lett.* **77** 5296
[32] Shengelaya A, Zhao G-M, Keller H, Muller K A and Kochelaev B I 2000 *Phys. Rev.* B **61** 5888
[33] Arulraj A, Gundakaram R, Biswas A, Gayathri N, Raychaudhuri A K and Rao C N R 1998 *J. Phys.: Condens. Matter* **10** 4447
[34] Raveau B, Maignan A, Martin C, Mahendiran R and Hervieu M 2000 *J. Solid State Chem.* **151** 330
[35] Chou F C, Belk N R, Kastner M A, Birgeneau R J and Aharony A 1995 *Phys. Rev. Lett.* **75** 2204
[36] Cai J-W, Wang C, Shen B-G, Zhao J-G and Zhan W-S 1997 *Appl. Phys. Lett.* **71** 1727
[37] Sun Y, Tong W, Xu X and Zhang Y 2001 *Phys. Rev.* B **63** 174438
[38] Pi L, Hebert S, Martin C, Maignan A and Raveau B 2003 *Phys. Rev.* B **67** 024430